Determination of wall shear stress from mean velocity and Reynolds shear stress profiles

Ralph J. Volino[1,*] and Michael P. Schultz[2,†]
[1]*Mechanical Engineering Department, United States Naval Academy, Annapolis, Maryland 21402, USA*
[2]*Naval Architecture and Ocean Engineering Department, United States Naval Academy, Annapolis, Maryland 21402, USA*

(Received 5 December 2017; published 22 March 2018)

An analytical method is presented for determining the Reynolds shear stress profile in steady, two-dimensional wall-bounded flows using the mean streamwise velocity. The method is then utilized with experimental data to determine the local wall shear stress. The procedure is applicable to flows on smooth and rough surfaces with arbitrary pressure gradients. It is based on the streamwise component of the boundary layer momentum equation, which is transformed into inner coordinates. The method requires velocity profiles from at least two streamwise locations, but the formulation of the momentum equation reduces the dependence on streamwise gradients. The method is verified through application to laminar flow solutions and turbulent DNS results from both zero and nonzero pressure gradient boundary layers. With strong favorable pressure gradients, the method is shown to be accurate for finding the wall shear stress in cases where the Clauser fit technique loses accuracy. The method is then applied to experimental data from the literature from zero pressure gradient studies on smooth and rough walls, and favorable and adverse pressure gradient cases on smooth walls. Data from very near the wall are not required for determination of the wall shear stress. Wall friction velocities obtained using the present method agree with those determined in the original studies, typically to within 2%.

DOI: 10.1103/PhysRevFluids.3.034606

I. INTRODUCTION

The wall shear stress, τ_w, expressed as a friction velocity, u_τ, or as a skin friction coefficient, c_f, is of fundamental interest for all wall-bounded flows. Flow velocities and lengths scale with u_τ in the inner region of the boundary layer, and the drag on surfaces is of practical interest. Although in principle straightforward, accurate determination of the local wall shear can in practice be difficult, and various methods have been developed to either directly measure or infer the skin friction. Winter [1], Haritonidis [2], and Klewicki *et al.* [3] are among those who provide reviews of some of the techniques available.

Direct measurement of the drag on a surface is possible with a floating element force balance, and if the sensor is sufficiently small relative to the size of the boundary layer, the local shear stress can be determined. Squire *et al.* [4] provide a recent example. Techniques utilizing microelectromechanical devices or oil film interferometry, as discussed by Naughton and Sheplak [5], are also based on direct responses to the wall shear. These techniques all have their challenges and limitations. Force balances, for example, can be expensive, require careful alignment with the surface to be accurate, and must

*volino@usna.edu
†mschultz@usna.edu

be moved and realigned if measurements are required at multiple locations. Oil film interferometry is not practical in liquid flows or on rough surfaces.

The wall shear stress is more commonly inferred from velocity measurements. For smooth walls, the wall shear is equal to the viscous shear at the wall, $\tau_w = \mu \frac{\partial U}{\partial y}|_{y=0}$, where μ is the dynamic viscosity, U is the mean streamwise component of the velocity, and y is the coordinate in the wall normal direction. Accurate determination of the velocity gradient at the wall can be possible if the boundary layer is sufficiently thick. Dixit and Ramesh [6], for example, used a surface hot wire probe (SHW) that was mounted in the wall and extended a known small distance from the surface. By keeping the wire within the viscous sublayer, it was effectively possible to measure the velocity gradient at the wall. As with the other methods discussed above, very near wall measurements are not always possible or practical, particularly when needed at multiple locations.

Other methods using velocity measurements typically rely on assumptions about the shape of the velocity profile farther from the wall. In zero pressure gradient (ZPG) turbulent boundary layers on smooth walls, the inner region of the mean streamwise velocity profile is self-similar in inner coordinates, and the Clauser fit technique [7] can be used to determine u_τ by fitting measured velocity profiles to the universal log law. The technique is well known to be accurate and requires only the streamwise velocity profile at the location of interest. With a shift of the universal log law, the Clauser fit technique can also be accurately applied to ZPG rough wall boundary layers, as demonstrated in studies such as Schultz and Flack [8]. Preston tubes, which measure the total pressure near the wall, typically extend beyond the viscous sublayer and rely on the same assumption of a universal log layer as the Clauser fit. Experiments and direct numerical simulations (DNS) such as those of Jones and Launder [9] and Spalart [10] show that the universal log layer is quite robust, even in mild to moderate non-ZPG boundary layers. With strong pressure gradients, however, significant deviations from the universal law of the wall are apparent, and straightforward applications of Clauser fit or Preston tube techniques lose accuracy.

The momentum deficit in a boundary layer results from the wall shear stress, so the skin friction can in principle be determined from the streamwise gradient of the momentum thickness, θ, using the momentum integral equation. The method does not presume a universal velocity profile, but it does require measurements at multiple streamwise locations to determine the streamwise evolution of θ. It is often subject to considerable uncertainty, however, as even small three-dimensional effects in a nominally two-dimensional boundary layer can result in significant error in $\partial\theta/\partial x$. The technique can produce good results, as demonstrated by Brzek *et al.* [11], who took great care to determine $\partial\theta/\partial x$ at closely spaced streamwise stations.

Several studies have considered the relationship between the Reynolds shear stress in the boundary layer and the wall shear. Included are Fukagata *et al.* [12], Deck *et al.* [13], Yoon *et al.* [14], and Renard *et al.* [15]. Mehdi and White [16] and Mehdi *et al.* [17] used the Reynolds shear stress and an integrated version of the momentum equation to determine the local skin friction based only on measurements at the streamwise location in question. Their method uses measured profiles of the mean velocity and the Reynolds shear stress, $-\overline{u'v'}$. The technique requires accurate estimates of the wall normal gradient of the total shear stress. Since the Reynolds shear stress is difficult to measure very near the wall, they used a fitting technique based on the expected shape of the total shear stress profile to smooth the experimental data and determine the gradient. The method was shown to work with ZPG boundary layer data from both smooth and rough walls. To the extent that the total shear stress depends on the pressure gradient, it is possible that the near wall fitting technique might require adjustment for non-ZPG cases.

Each of the methods described above has been successfully used. Each also has its challenges and limitations. The present paper presents a new method based on the momentum equation that does not require assumptions about the shape of the mean velocity profile or otherwise rely on fitting of experimental data to expected functions. It presumes a steady, two-dimensional boundary layer, but can otherwise be used in flows with arbitrary pressure gradients and surface roughness. It utilizes profiles of the mean velocity and Reynolds shear stress but does not require $-\overline{u'v'}$ data from very

near the wall. The formulation attempts to minimize dependence on streamwise gradients, but some dependence remains, making data from two or more streamwise locations necessary and the process of determining the wall shear iterative.

In the following sections, an analytical method is developed for computing the Reynolds shear stress profile based on the mean streamwise velocity profile. This method is verified using solutions from laminar boundary layers and turbulent DNS data. It is then applied to experimental data from the literature from boundary layers on smooth and rough surfaces with both zero and nonzero pressure gradients to determine the local wall shear stress.

II. ANALYSIS

The Reynolds-averaged, streamwise momentum equation for two-dimensional, steady boundary layers with constant properties, is

$$U\frac{\partial U}{\partial x}+V\frac{\partial U}{\partial y}-\frac{\partial(\tau/\rho)}{\partial y}+\frac{1}{\rho}\frac{dP}{dx}+\frac{\partial\overline{u'^2}}{\partial x}=0, \tag{1}$$

where x and y are the streamwise and wall normal coordinate directions, U and V are the respective mean velocities in these directions, ρ is the density and P is the static pressure. The total stress, $\tau=-\rho\overline{u'v'}+\mu\frac{\partial U}{\partial y}$, is the sum of the Reynolds shear stress and the viscous stress. The Reynolds normal stress term, $\partial\overline{u'^2}/\partial x$, is typically small and is neglected, but is kept here for completeness. Next, the continuity equation is used to substitute for V, with the assumption that $V=0$ at the wall:

$$U\frac{\partial U}{\partial x}-\int\frac{\partial U}{\partial x}\,dy\frac{\partial U}{\partial y}-\frac{\partial(\tau/\rho)}{\partial y}+\frac{1}{\rho}\frac{dP}{dx}+\frac{\partial\overline{u'^2}}{\partial x}=0. \tag{2}$$

The equation is now integrated in the wall normal direction to solve for τ at an arbitrary location y:

$$\frac{\tau}{\rho}=\frac{\tau_w}{\rho}+\frac{1}{\rho}\frac{dP}{dx}y-U\int_0^y\frac{\partial U}{\partial x}\,dy+2\int_0^y U\frac{\partial U}{\partial x}\,dy+\int_0^y\frac{\partial\overline{u'^2}}{\partial x}\,dy. \tag{3}$$

Equation (3) could in principle be used to solve for τ_w using the steamwise velocity profile and the measured Reynolds shear stress at an arbitrary y location. An example is provided by Brzek *et al.* [11], who used this method for a ZPG profile and showed that the wall shear obtained agreed well with the result obtained from the momentum integral method. Difficulties can arise with this procedure, however. There are two options for applying Eq. (3). If a location for analysis is chosen very near the wall, the Couette flow assumption states that the streamwise gradients are negligible. This eliminates the last three terms in Eq. (3). The pressure gradient term is assumed known, but the total stress, τ, must be extracted from the experimental data. This is problematic, since the Reynolds shear stress is inherently difficult to measure very close to the wall. The alternative approach is to use a y location farther from the wall, where τ is more readily obtained. The Couette flow assumption no longer applies, however, so the partial derivative $\partial U/\partial x$ at fixed y becomes non-negligible, as will be demonstrated in the sections below. While $\partial U/\partial x$ can be approximated from data at two streamwise locations, this typically brings with it added uncertainty, particularly in non-ZPG cases where $\partial U/\partial x$ can become significant even close to the wall.

The development through Eq. (3) is common to other studies. It is essentially the same as Eq. (3) of Brzek *et al.* [11]. The difference between methods is in the subsequent development. Mehdi *et al.* [17], for example, begin with the streamwise momentum equation [Eq. (1)], and integrate it three times in the wall normal direction. The resulting equation only requires profile data of the mean velocity and Reynolds shear stress at a single streamwise location to determine the wall shear. As noted above, it requires the wall normal gradient of the total shear, which typically requires assumptions about the profile shape to determine with sufficient accuracy. As another example, Brzek *et al.* [11] and others before them integrated Eq. (3) to obtain the momentum integral equation. As noted above, this

approach requires only mean velocity profile data, but at multiple streamwise locations. It depends on an ability to accurately compute the streamwise gradient of the momentum thickness. The present paper takes a new and different approach, transforming Eq. (3) into wall coordinates and separating terms which depend on streamwise gradients from those which do not. It requires mean velocity and Reynolds shear stress profiles from at least two streamwise stations, but seeks to minimize the dependence on streamwise gradients from that required in Eq. (3).

For the present method, to reduce the dependence on the $\partial U/\partial x$ terms, Eq. (3) is transformed from $x - y$ to $x - y^+$ coordinates, and made dimensionless. The standard definitions

$$y^+ = \frac{y u_\tau}{\nu}, \quad U^+ = \frac{U}{u_\tau}, \quad \overline{u'v'}^+ = \frac{\overline{u'v'}}{u_\tau^2}, \quad \overline{u'^2}^+ = \frac{\overline{u'^2}}{u_\tau^2}, \quad \frac{1}{\rho}\frac{dP}{dx} = -\frac{K U_e^3}{\nu}, \quad \frac{c_f}{2} = \left(\frac{u_\tau}{U_e}\right)^2$$

are used where U_e is the local freestream velocity, ν is the kinematic viscosity, and K is the acceleration parameter:

$$K = \frac{\nu}{U_e^2}\frac{dU_e}{dx}.$$

The resulting equation is

$$\begin{aligned}
-\overline{u'v'}^+ = 1 &- \underbrace{\frac{\partial U^+}{\partial y^+}}_{I} - \underbrace{\frac{K}{(c_f/2)^{3/2}} y^+}_{II} + \underbrace{\left[\frac{K}{\sqrt{c_f/2}} + \frac{\nu}{U_e(c_f/2)}\frac{d\sqrt{c_f/2}}{dx}\right]\int_0^{y^+} U^{+^2}\, dy^+}_{III} \\
&+ \underbrace{\frac{\nu}{U_e\sqrt{c_f/2}}\left(2\int_0^{y^+} U^+\frac{\partial U^+}{\partial x} dy^+ - U^+\int_0^{y^+}\frac{\partial U^+}{\partial x}\, dy^+\right)}_{IV} \\
&+ \underbrace{\left[\frac{K}{\sqrt{c_f/2}} + \frac{\nu}{U_e(c_f/2)}\frac{d\sqrt{c_f/2}}{dx}\right]\left(y^+\overline{u'^2}^+ + \int_0^{y^+}\overline{u'^2}^+\, dy^+\right)}_{V} \\
&+ \underbrace{\frac{\nu}{U_e\sqrt{c_f/2}}\int_0^{y^+}\frac{\partial \overline{u'^2}^+}{\partial x}\, dy^+}_{VI}.
\end{aligned} \tag{4}$$

The left side of Eq. (4) is the dimensionless Reynolds shear stress term. The terms on the right side depend only on the streamwise velocity profile. Term I is the viscous shear stress term and term II is the pressure gradient term. Terms III and IV result from the integrals of $\partial U/\partial x$ in Eq. (3), and have been divided into a term which depends on the streamwise gradient $\partial U^+/\partial x$ (term IV), and a term which does not (term III). Terms V and VI result from the integral of the streamwise gradient of the streamwise Reynolds normal stress in Eq. (3) and have again been divided into a term that depends on the streamwise gradient (term VI) and a term that does not (term V). Terms V and VI are typically small throughout the boundary layer, and were found to be unhelpful for the experimental cases considered in this paper. They are not included in the comparisons below, except to assess their magnitude with DNS data.

After the coordinate transformation from Eq. (3) to Eq. (4), the streamwise gradients are evaluated with y^+ held constant. Unlike $\partial U/\partial x$ at constant y, which typically becomes significant in the buffer layer or inner part of the log layer, $\partial U^+/\partial x$ at constant y^+ is nearly zero from the wall to the outer edge of the log layer for the ZPG boundary layer, and only becomes significant in the wake. As will be shown below, $\partial U^+/\partial x$ is also typically small for much of the inner part of the boundary layer even when inner region self-similarity and the law of the wall do not strictly hold, such as for non-ZPG cases. Term III becomes important when $\partial U/\partial x$ at constant y becomes significant, which typically

occurs for $y/\delta \gtrsim 0.1$ (δ being the 99% boundary layer thickness). Term IV, in contrast, only becomes important when $\partial U^+/\partial x$ at constant y^+ becomes significant, so it is typically negligible for the inner third of the boundary layer. Hence the need to compute the streamwise gradient of the mean velocity for much of the boundary layer is less with the formulation of Eq. (4) than with that of Eq. (3).

Equation (4) is used to find u_τ by calculating the terms on the right side of the equation using the mean velocity profile and plotting the result against the measured dimensionless Reynolds shear stress. The u_τ selected is the one that provides the best fit of the data. Since Eq. (4) is an implicit equation for the wall shear, the entire process is iterative due to the presence of c_f on the right side, in particular the $d\sqrt{c_f/2}/dx$ term in the coefficient of term III and in $\partial U^+/\partial x$ in term IV. The process for finding u_τ is shown with a flow chart in the Appendix and includes the following steps: (1) Mean velocity and Reynolds shear stress profiles are acquired at two or more streamwise locations. (2) A guess is made for u_τ at each streamwise station. The guess need only be physically plausible; accuracy is not required. Simply assuming $u_\tau = 0.05U_e$ at each station is adequate. (3) The u_τ values are then made dimensionless as c_f, and these are used to compute $d\sqrt{c_f/2}/dx$ at each station. The dimensional data at each station are then converted to wall coordinates using the u_τ values. (4) Profiles of $\partial U^+/\partial x$ at constant y^+ are next evaluated at each station using data from neighboring stations. (5) Next, the fitting is done at the first station. The terms on the right side of Eq. (4) are computed at all y^+ locations and plotted against the $\overline{u'v'}^+$ profile. If it appears that the fit to the $\overline{u'v'}^+$ profile can be improved, a new u_τ is chosen and used to reevaluate c_f and reconvert the measured dimensional data to wall coordinates at the station in question. Equation (4) is revaluated and plotted. Iteration on step (5) is continued until the fit is judged as good as attainable. (6) The process of step (5) is repeated for all other streamwise stations. (7) If u_τ has changed at any station after step (3), steps (3)–(7) are repeated. When u_τ stops changing, the process is complete. About three iterations are needed to fit the data as well as possible at all stations. It should be noted that the fit of Eq. (4) may not be perfect due to experimental uncertainty and the approximations required for the derivatives $d\sqrt{c_f/2}/dx$ and $\partial U^+/\partial x$. There is freedom, however, to deemphasize the fit very near the wall where $\overline{u'v'}^+$ uncertainty is high, or in the outer region where term IV is important, and instead focus on the middle of the boundary layer where confidence in all terms is higher.

As a modification to the method above, the term $d\sqrt{c_f/2}/dx$ can be treated as an independent parameter in the fitting. Any error in $d\sqrt{c_f/2}/dx$ will change not only the magnitude of the computed profile, but also the shape of the profile in the region where Term III of Eq. (4) is significant. By adjusting both u_τ and $d\sqrt{c_f/2}/dx$ when doing the fitting, it can become possible to match the computed profile to the $\overline{u'v'}^+$ data over a wider range of y locations. A fit of more of the profile can provide more confidence in the determination of u_τ. Varying $d\sqrt{c_f/2}/dx$ might be considered analogous to including a y shift when using the Clauser plot method to account for uncertainty in the location of the wall. The location of the wall is known at least approximately, so any y shift imposed to improve the Clauser fit should be within the uncertainty. Similarly, for the present method $d\sqrt{c_f/2}/dx$ is known at least approximately based on the c_f values at neighboring stations, so any adjustment of its value should be within its estimated uncertainty. No such adjustment of $d\sqrt{c_f/2}/dx$ was used in the determination of u_τ for any of the cases in the present paper but the technique was tested and found to be potentially useful if applied judiciously.

III. LAMINAR SOLUTIONS

The formulation of Eq. (4) can be tested and the significance of the various terms examined using flows with known exact solutions, such as laminar Falkner and Skan [18] wedge flows with $U_e = Cx^m$. Since the turbulent shear is zero, Eq. (4) is solved for the laminar shear stress (term I) and converted to laminar similarity coordinates using the following definitions:

$$\eta = \frac{y}{\sqrt{\nu x/U_e}}, \quad \varsigma'(\eta) = \frac{U}{U_e}.$$

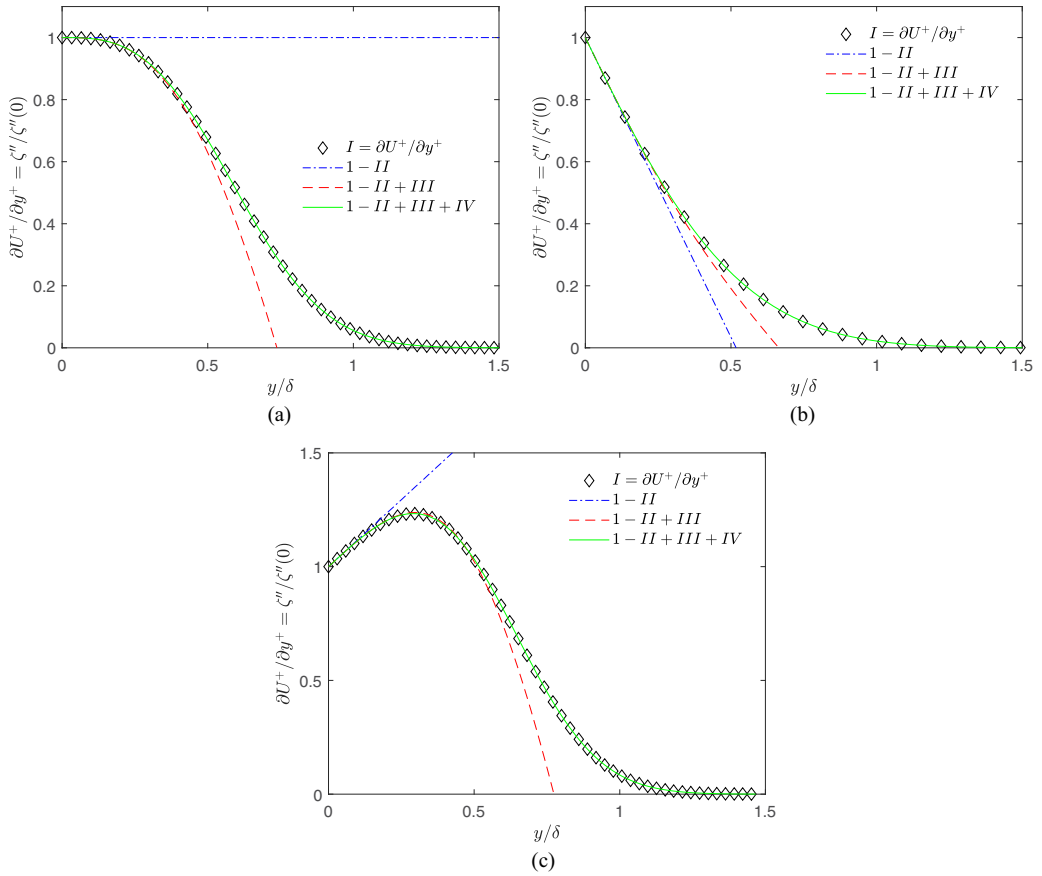

FIG. 1. Terms of Eq. (5) as indicated in legend for laminar Falkner and Skan [18] boundary layer, (a) ZPG with $m = 0, \varsigma'' = 0.332$; (b) FPG with $m = 1$, $\varsigma'' = 1.232$; (c) APG with $m = -0.0476$, $\varsigma'' = 0.221$.

The resulting equation is

$$\underbrace{\frac{\varsigma''}{\varsigma''(0)}}_{I} = 1 - \underbrace{\frac{m\eta}{\varsigma''(0)}}_{II} + \underbrace{\frac{3m-1}{4\varsigma''(0)}\int_0^\eta \varsigma'^2\, d\eta}_{III} + \underbrace{\frac{m+1}{4\varsigma''(0)}\left[2\int_0^\eta (\varsigma'^2 - \eta\varsigma'\varsigma'')\, d\eta + \varsigma'\int_0^\eta \eta\varsigma''\, d\eta - \varsigma'\varsigma\right]}_{IV} \tag{5}$$

with terms I–IV in Eq. (5) corresponding to those in Eq. (4). Equation (5) is applicable for any value of m between -0.09 (separation) and $+\infty$. The importance of the terms in the equation is shown next for example cases with zero, favorable, and adverse pressure gradients. The ZPG case is the Blasius boundary layer with $m = 0$ and $\varsigma''(0) = 0.332$, and is shown in Fig. 1(a). The viscous shear stress (term I) is shown with symbols and successive approximations to it using the terms on the right side of Eq. (5) are shown with lines. Term II is zero for the ZPG case, so the first approximation is unity, which agrees with the viscous shear to about $y/\delta = 0.1$. This is the constant stress region. Including term III extends the agreement to about $y/\delta = 0.35$, with the difference from the viscous shear remaining small until $y/\delta > 0.5$. With term IV included, the match to the viscous shear is exact

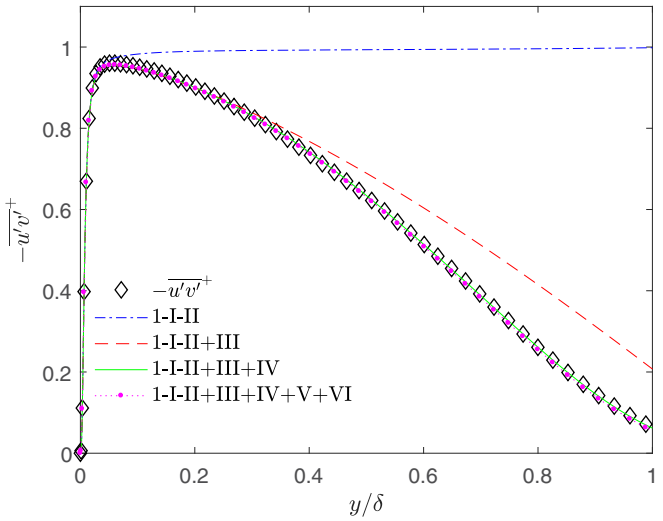

FIG. 2. Terms of Eq. (4) as indicated for turbulent ZPG DNS of Sillero *et al.* [20], $\mathrm{Re}_\theta = 4500$, $\mathrm{Re}_\tau = 1437$.

for the full boundary layer, which is expected since Eqs. (4) and (5) are equivalent to Eq. (1) with no additional assumptions or approximations.

Figure 1(b) shows a favorable pressure gradient (FPG) example with $m = 1$ and $\varsigma''(0) = 1.232$. The inclusion of term II provides a good approximation of the laminar shear near the wall, as in the ZPG case the addition of term III extends the agreement toward the middle of the boundary layer, and including term IV produces exact agreement. The same can be seen for an adverse pressure gradient (APG) case with $m = -0.0476$ and $\varsigma''(0) = 0.221$ in Fig. 1(c).

IV. TURBULENT DNS

The terms of Eq. (4) are considered for a turbulent boundary layer using the ZPG DNS results of Jiménez *et al.* [19] and Sillero *et al.* [20]. Tabulated velocity profile data were provided from the DNS database at discrete momentum thickness Reynolds numbers, Re_θ, of 1100, 1151, 1968, and 4000–6000 in increments of 500. Results for c_f were provided at more closely spaced locations, so $d\sqrt{c_f/2}/dx$ could be determined very accurately. The $\partial U^+/\partial x$ values for term IV of Eq. (4) were approximated as $\Delta U^+/\Delta x$ using the differences between values at equal y^+ at adjacent profile stations. Equation (4) was fit to the DNS profile data at all available Reynolds numbers. The u_τ values determined from the fit exactly matched those obtained from the velocity gradient at the wall. Figure 2 shows a typical result for $\mathrm{Re}_\theta = 4500$ ($\mathrm{Re}_\tau = \delta^+ = \delta u_\tau/\nu = 1437$). The $-\overline{u'v'}^+$ data from the DNS are shown with symbols, and the terms from the right side of Eq. (4) are shown with lines. Using only the laminar shear stress term (I), there is agreement with the Reynolds shear stress from the wall to about $y/\delta = 0.05$. This is the constant stress region. Term II contributes nothing because the pressure gradient is zero. Adding term III extends the agreement to about $y/\delta = 0.35$. Although there was some approximation in $\partial U^+/\partial x$ due to the discrete spacing of the mean profile stations, the addition of term IV results in good agreement with the Reynolds shear stress data to the edge of the boundary layer. Adding terms V and VI of Eq. (4) results in a very slight shift of the profile, with a maximum change of about 0.006 in $\overline{u'v'}^+$. This confirms that terms V and VI are not typically significant for ZPG cases.

As noted above, terms III and IV in Eq. (4) result from the streamwise integral of $\partial U/\partial x$ in Eq. (3). The emergence of term III in Fig. 2 shows that $\partial U/\partial x$ at constant y becomes significant for $y/\delta > 0.05$. Term IV does not become significant until $\partial U^+/\partial x$ at constant y^+ becomes significant

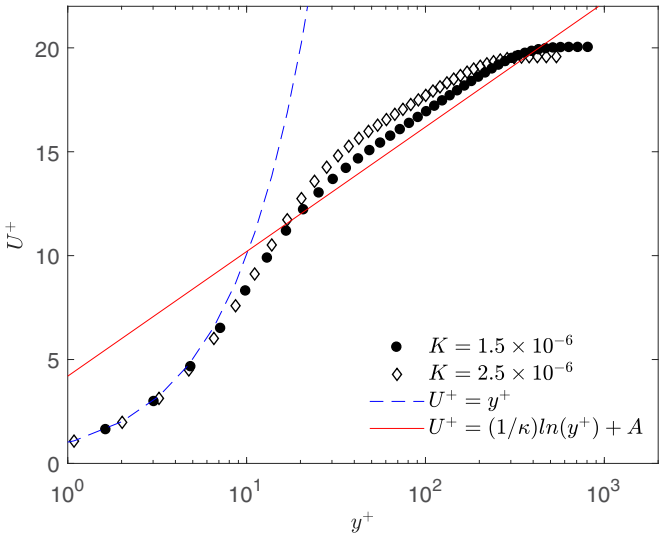

FIG. 3. Mean velocity profiles for FPG sink flow DNS of Spalart [10], log law constants $\kappa = 0.384$, $A = 4.2$.

for $y/\delta > 0.35$. Hence, the transformation from Eq. (3) to Eq. (4) removed the need to accurately compute the streamwise gradient of the mean velocity for the region between $y/\delta = 0.05$ and 0.35 for this profile.

The equilibrium sink flow DNS cases of Spalart [10] provide another test of the present method. The mean velocity is shown in inner coordinates in Fig. 3. The strong FPG causes deviation from the universal law of the wall. If a Clauser fit were used to force a match to the universal log law, u_τ would be predicted about 5% too high for the $K = 1.5 \times 10^{-6}$ case and about 9% too high for the $K = 2.5 \times 10^{-6}$ case. The method of the present paper avoids this problem. For the equilibrium sink flow, c_f and Re_θ are constants, and the full boundary layer exhibits similarity in both inner and outer coordinates. This means that $d\sqrt{c_f/2}/dx$ and $\partial U^+/\partial x$ are zero, simplifying the coefficient of term III in Eq. (4) and eliminating term IV [note that if Eq. (3) were used, it would still be necessary to compute $\partial U/\partial x$ at constant y, and that the term would be large due to the acceleration]. Figure 4 shows the fit of the data for the $K = 2.5 \times 10^{-6}$ case. With the FPG, there is no constant stress region. The total stress drops rapidly from its value of 1 at the wall. Terms I and II match $-\overline{u'v'}^+$ to about $y/\delta = 0.05$. With term III included, the match is good for the entire boundary layer. The addition of term V (term VI is identically zero for the sink flow) improves the match to nearly perfect. Term V adds about 0.014 to the right side of Eq. (4), indicating that for strong FPG cases, it may be worth considering if it can be computed accurately, but it is still small and can be neglected with only a minor effect.

V. EFFECTS OF MISSING OR UNCERTAIN DATA

The results above demonstrate that with exact laminar solutions or essentially perfect DNS data, the fitting of Eq. (4) is equally perfect when all terms are included. This is expected since Eq. (4) is an exact formulation of the momentum equation. The question arises, however, of how accurately u_τ can be determined when experimental data are missing from the near wall region or experimental uncertainty is present in the data that are available. This is shown in Sec. VI through application of the method to experimental results, but is considered in a more controlled manner next by removing data and adding errors to the DNS results.

Acquisition of experimental data near a wall is limited by the size and resolution of the probes used to obtain the data. Resolving the near wall flow can be particularly difficult with particle image

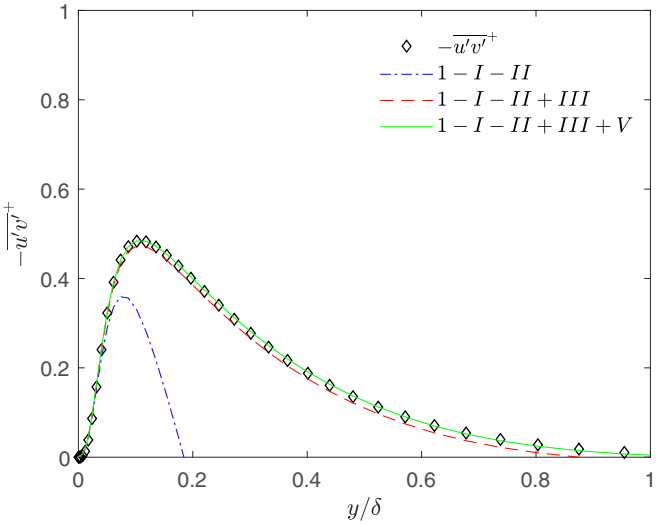

FIG. 4. Terms of Eq. (4) as indicated in legend for turbulent FPG sink flow DNS of Spalart [10], $K = 2.5 \times 10^{-6}$, $\mathrm{Re}_\theta = 415$, $\mathrm{Re}_\tau = 253$.

velocimetry. To simulate this, data were removed from the near wall region of the DNS cases of Figs. 2 and 4. This affects the computation of the integrals in Eq. (4), and requires an approximation of the contribution from the near wall region. Three potential approximations for the integral in term III are given in the following equations, with y_c denoting the closest remaining data location to the wall:

$$\int_0^{y^+} U^{+^2} dy^+ \approx \int_{y_c^+}^{y^+} U^{+^2} dy^+ \tag{6}$$

$$\int_0^{y^+} U^{+^2} dy^+ \approx U^{+^2}_{y=y_c} \frac{y_c}{2} + \int_{y_c^+}^{y^+} U^{+^2} dy^+, \tag{7}$$

$$\int_0^{y^+} U^{+^2} dy^+ \approx \frac{7}{9} C^2 y_c^{+^{9/7}} + \int_{y_c^+}^{y^+} U^{+^2} dy^+. \tag{8}$$

Equation (6) ignores the contribution from the near wall region, which is equivalent to assuming the integrand is zero for $y < y_c$. Equation (7) uses the trapezoidal rule to numerically integrate from the value of the integrand at the wall (zero in this case) to the value at y_c. Equation (8) assumes a mean velocity profile shape for the near wall region, $U^+ = C y^{+^{1/7}}$, and integrates this function from the wall to y_c. The constant C is evaluated using the data point at y_c as $C = U^+_{y=y_c}/y_c^{+^{1/7}}$. Approximations are also needed for the integrals in term IV (and terms V and VI if used), but the effects of these approximation are negligible since the integrands are near zero for the inner part of the boundary layer. The equivalent of Eq. (7) was used for the term IV approximations. Equations (6)–(8) are intended as potentially useful approximations for the near wall region, even if they are not necessarily based on accurate models of the mean velocity. For the ZPG case, Eq. (7) under predicts the mean velocity, Eq. (6) under predicts it more, and Eq. (8) overpredicts it. The effects of the approximations for the profile of Fig. 2 are shown in Fig. 5 for $y_c/\delta = 0.4$. All quantities shown in Fig. 5 were computed using the correct value of u_τ obtained from the DNS. The lines in the figure were computed using terms I–IV of Eq. (4). With the approximation of Eq. (6), noticeable error is observed. If u_τ were adjusted to fit the Eq. (6) approximation to the $-\overline{u'v'}^+$ data, u_τ would be

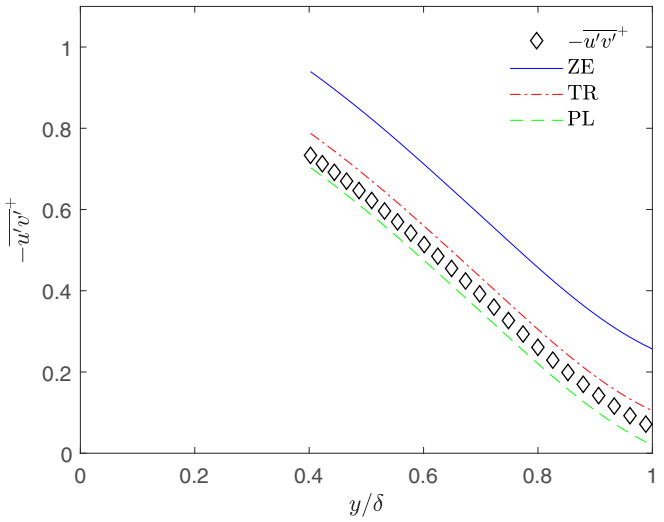

FIG. 5. Fit to data of Fig. 2 truncated at $y_c/\delta = 0.4$ using terms 1-I-II+III+IV with approximations of equations indicated [ZE (zero): Eq. (6); TR (trapezoidal rule): Eq. (7); PL (power law): Eq. (8)] for the near wall region.

under predicted by 13.5%. If the fitting were done using Eq. (7), the underprediction in u_τ would be reduced to 2.6%. Using Eq. (8), u_τ would be overpredicted by 1.7%.

Figure 6(a) shows the error introduced in u_τ as a function of the extent of the missing data for the profile of Fig. 2. With the crude approximation of Eq. (6), the error is less than 2% when $y_c/\delta < 0.1$, but increases to 20% when $y_c/\delta = 0.5$. With the simple approximation of Eq. (7), the error remains below 2% for y_c/δ up to about 0.3, and is still below 5% for $y_c/\delta = 0.6$. For the power law approximation of Eq. (8), the error remains below 1% to $y_c/\delta = 0.3$, and remains below 3% even when data are removed from $y/\delta < 0.8$. The log region of this boundary layer extends to $y^+ \approx 270$, which corresponds to $y/\delta \approx 0.2$. The results of Fig. 6 indicate that the present method can be useful even when data are absent from the log region and only available in the outer part of the wake. Figure 6(b) shows results for the FPG case of Fig. 4. Term III of Eq. (4) is larger for the FPG case than for the ZPG, causing the errors to grow more rapidly as y_c increases. Using Eq. (7),

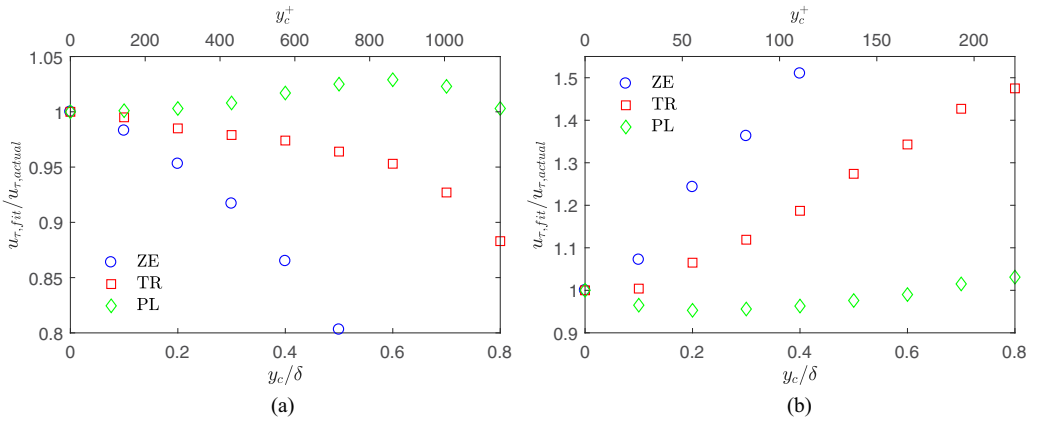

FIG. 6. Ratio of of u_τ determined with data truncated inside y_c/δ using equations indicated [ZE: Eq. (6); TR: Eq. (7); PL: Eq. (8)] for near wall region to u_τ from DNS, (a) ZPG case of Fig. 2, (b) FPG case of Fig. 4.

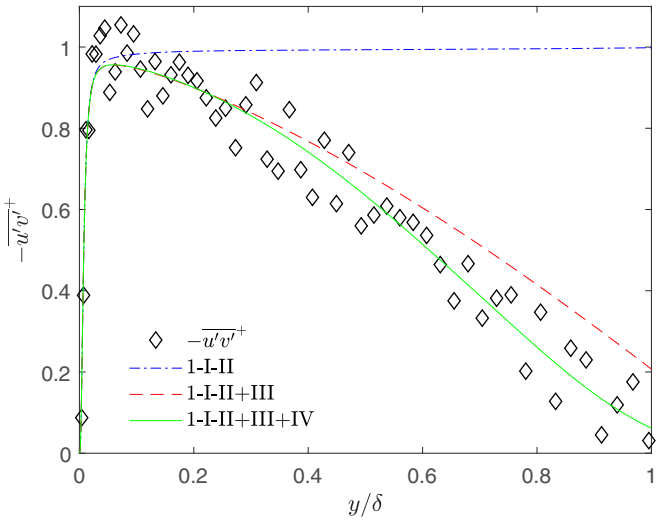

FIG. 7. Profile of Fig. 2 with Gaussian noise added to $-\overline{u'v'}^+$.

the error remains below 0.5% to $y_c/\delta = 0.1$, but then rises steadily as more data are removed. Using Eq. (8), the error in u_τ remains below 4.7% for all y_c/δ. The 1/7 power law of Eq. (8) was chosen because it is commonly used as a simple approximation to the mean velocity profile. One could use a better approximation for the inner region and reduce the error further.

Experimental uncertainty is another potential source of error in u_τ. Gaussian noise was added to the quantities in Eq. (4) of the DNS results of Figs. 2 and 4. Even large amounts of noise added to U^+ and $\partial U^+/\partial x$ had little effect on terms III and IV, since it was averaged to near zero in the integrals. The noise in U^+ was, however, carried through into the viscous shear (term I), so a sufficient quantity of data should be acquired to produce a smooth U^+ profile. Figure 7 shows the effect of Gaussian noise added to $-\overline{u'v'}$ for the profile of Fig. 2. The amplitude of the noise was $\pm 10\%$ of the maximum $-\overline{u'v'}$ in the profile. If the fitting is done though the center of the scattered data, no error is added to u_τ. If the fitting is done at the edges of the scatter, an error of 3% results.

Bias error in the measured quantities also affects u_τ. A 5% bias in the mean velocity, which would be large in most experiments, results in less than a 1% error in u_τ. Error in u_τ is proportional to any bias in the Reynolds shear, with a 5% bias in $-\overline{u'v'}$ resulting in a 2.5% error in u_τ. The streamwise gradient $\partial U^+/\partial x$ could be subject to considerable error, depending on the streamwise spacing of the measurement stations, and this error is proportional to the error in term IV of Eq. (4). For the profile of Fig. 2, term IV makes no significant contribution for $y/\delta < 0.3$, so errors in $\partial U^+/\partial x$ would have no effect in this region. If the fitting of the data were focused at $y/\delta = 0.4$, a 20% bias in $\partial U^+/\partial x$ would result in about a 0.25% error in u_τ. If the fit were focused at $y/\delta = 0.6$, the same 20% bias would cause a 1% error in u_τ. Hence, at least for the profile of Fig. 2, accurate determination of $\partial U^+/\partial x$ does not appear to be critical, even if data are not available close to the wall. It is best, however, to use data from as close to the wall as possible, to reduce the reliance on this term.

Another potential source of error results from the estimation of the gradient of the skin friction coefficient, $d\sqrt{c_f/2}/dx$. For the ZPG case, any error in this term results in the same percentage error in term III of Eq. (4). For the profile of Fig. 2, a 10% error in $d\sqrt{c_f/2}/dx$ would result in a 0.5% error in u_τ if the profile fit were focused at $y/\delta = 0.2$, and 1%, 2%, and 2.8% errors for fits focused at $y/\delta = 0.4$, 0.6, and 0.8, respectively. The size of the error in u_τ scales linearly with the error in $d\sqrt{c_f/2}/dx$, so, for example, a 40% error in $d\sqrt{c_f/2}/dx$ would cause a 2% error in u_τ if the fit were done at $y/\delta = 0.2$. As noted above, an estimate of u_τ can be produced using data at large y/δ,

TABLE I. Iterations to find u_τ for $U_e = 15.2$ m/s smooth wall case of Morrill-Winter *et al.* [21] and comparison of present method to Clauser fit.

x [m]	u_τ [m/s] Guess	u_τ [m/s] 1st it.	u_τ [m/s] 2nd it.	u_τ [m/s] 3rd it.	u_τ [m/s] Clauser	Difference [%]
4.5	0.6	0.545	0.545	0.545	0.541	0.7
7.0	0.6	0.515	0.518	0.518	0.519	−0.2
11.9	0.6	0.510	0.512	0.512	0.512	0
18.0	0.6	0.500	0.498	0.500	0.497	0.6

but the uncertainty is reduced if data are available closer to the wall where the importance of terms III and IV are lower.

The combined uncertainty in u_τ results from all of the factors described. For the cases considered above, the absence of near wall data and the bias uncertainties in $-\overline{u'v'}$, $d\sqrt{c_f/2}/dx$, and $\partial U^+/\partial x$ were most significant. If data were available at $y/\delta = 0.1$ or closer, the dominant uncertainty would be from the Reynolds shear stress, and the percentage uncertainty in u_τ would be about half that in $-\overline{u'v'}$. If data were only available for $y/\delta \geqslant 0.2$, the uncertainty in $d\sqrt{c_f/2}/dx$ would become an additional source of noticeable error. For $y_c/\delta > 0.4$, the effect of $\partial U^+/\partial x$ would become important. The magnitude of these uncertainties would depend on the details of particular experiments. As an example using the profile of Fig. 2, if $y_c/\delta = 0.2$ and the errors in $-\overline{u'v'}$, $d\sqrt{c_f/2}/dx$, and $\partial U^+/\partial x$ were 5%, 20%, and 20%, respectively, the error in u_τ could be as high as 3.4%. This is in the worst case with all of the errors biased in the same direction. For $y_c/\delta = 0.4$ with the same errors in the input quantities, the error in u_τ would be 6%. This is a significant error, but it should be remembered that it occurs when there are no data in the inner 40% of the boundary layer. It is doubtful that any technique for finding u_τ could do better under these circumstances. The Clauser fit would be useless since there would be no data in the log region.

VI. EXPERIMENTAL DATA

The present method is next used to extract the wall shear stress from experimental data. This is considered first for the ZPG boundary layer on a smooth wall using the data of Morrill-Winter *et al.* [21]. The data were acquired in large wind tunnels at the University of Melbourne and the University of New Hampshire using miniature multi-element hot-wire probes. Both facilities have trips followed by very long test sections, resulting in thick boundary layers that facilitate measurements at small y^+. The full iterative procedure was used to determine u_τ at each streamwise measurement station for each experimental case. The initial estimates for u_τ could be set as the square root of the maximum $-\overline{u'v'}$ in each profile or estimated with a Clauser fit. As an exercise to demonstrate that the initial guess is not critical, u_τ was set to 0.6 m/s at all stations for a case from the Melbourne wind tunnel with $U_e = 15$ m/s. This 0.6 value was based on a guess that U_e/u_τ would be about 25. Results showing the iterations for this case are given in Table I. Also shown are the differences between u_τ found by the present method and the values determined by Morrill-Winter *et al.* [21] using Clauser fits. The differences averaged 0.4% and were at most 0.7%. Results from the present method and the Clauser fit for all of the stations and cases of Morrill-Winter *et al.* [21] are given in Table II, again showing good agreement between the two methods.

A typical fit of the data is shown in Fig. 8 for the streamwise station at $x = 11.9$ m downstream of the trip. The constant stress region extends to about $y/\delta = 0.04$, as in the DNS results of Fig. 2. Including term III allows a good fit of the data to about $y/\delta = 0.2$. With term IV included, the region of good fit is extended to about $y/\delta = 0.4$. Because of the very thick boundary layer, good Reynolds shear stress data were available at low y/δ, making it possible to determine u_τ using only the constant stress region. In a smaller facility where such data were not available, the present method would allow evaluation of u_τ using data considerably farther from the wall. The sensitivity of the fit to the choice

TABLE II. Comparison of u_τ found with present method and Clauser fit for smooth wall ZPG cases of Morrill-Winter *et al.* [21] from Melbourne (M) and New Hampshire (NH).

Facility	U_e [m/s]	x [m]	δ^+	u_τ [m/s] Present	u_τ [m/s] Clauser	Difference [%]
M	10.1	4.5	2048	0.370	0.368	0.5
M	10.1	7.0	2662	0.357	0.356	0.3
M	10.0	11.9	4093	0.339	0.340	−0.3
M	10.0	18.0	5718	0.334	0.334	0
M	15.2	4.5	2993	0.545	0.541	0.7
M	15.1	7.0	3860	0.518	0.519	−0.2
M	15.3	11.9	5963	0.512	0.512	0
M	15.3	18.0	8038	0.500	0.497	0.6
NH	4.4	16.0	2870	0.156	0.156	0
NH	4.2	34.1	4997	0.144	0.144	0
NH	4.3	66.1	7334	0.144	0.144	0
NH	6.6	16.0	3771	0.230	0.230	0
NH	6.6	33.9	6457	0.218	0.220	−0.9
NH	6.6	66.0	10102	0.213	0.215	−0.9
NH	8.8	16.0	4951	0.299	0.301	−0.7
NH	8.8	34.0	7485	0.291	0.293	−0.7
NH	8.8	66.0	12701	0.281	0.285	−1.4

of u_τ is shown in Figs. 9 and 10. In Fig. 9 the value of u_τ is varied by $\pm 1\%$ from the value in Fig. 8. Although the fit appears better in Fig. 8, one might argue for one of the values used in Fig. 9 depending on which part of the profile was emphasized in the fitting. Figure 10 shows the fit with u_τ varied by $\pm 3\%$ from the value in Fig. 8. Clearly the fits in Fig. 10 are not as good as in Figs. 8 or 9, showing that the fitting of u_τ has a resolution of about 1%. To further check this resolution, the full fitting procedure was independently done by both of the present authors for all of the cases of Morrill-Winter *et al.* [21]. The average difference in u_τ at any measurement location was 0.24% with a maximum of 0.7%.

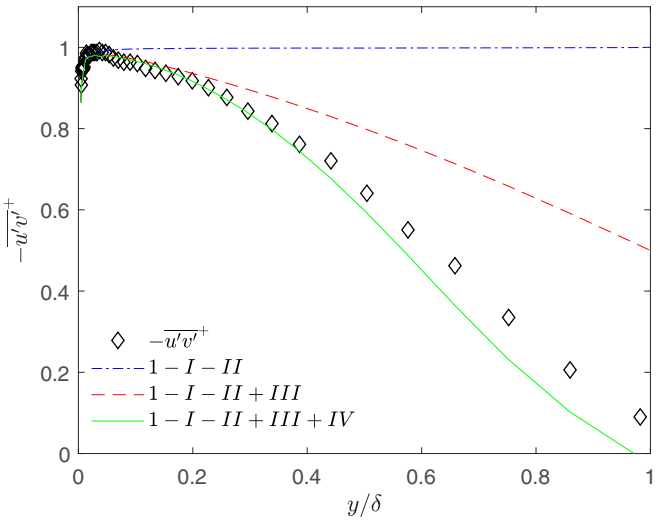

FIG. 8. Terms of Eq. (4) as indicated in legend for turbulent smooth wall ZPG flow of Morrill-Winter *et al.* [21], $x = 11.9\,\mathrm{m}$, $U_e = 15.3\,\mathrm{m/s}$, $\delta^+ = 5963$, $u_\tau = 0.512\,\mathrm{m/s}$.

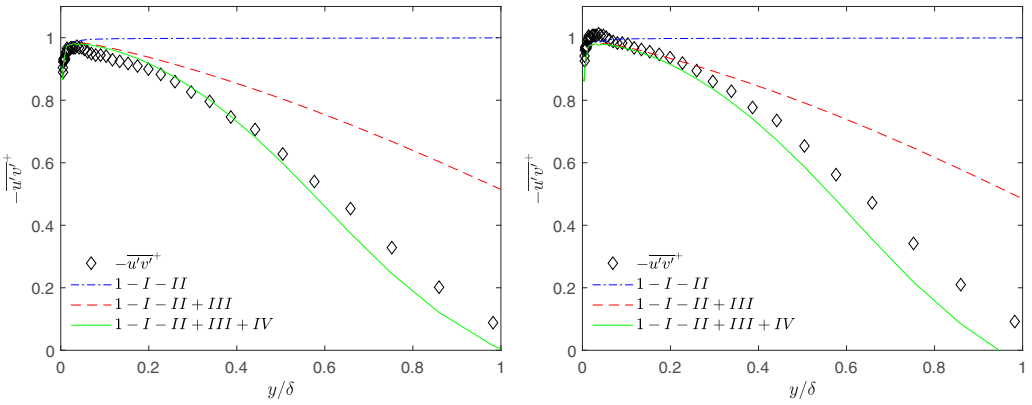

FIG. 9. Case of Fig. 8 with u_τ (a) increased by 1%, (b) decreased by 1%.

Experiments on a ZPG rough-wall boundary layer were conducted by Squire *et al.* [4] and Morrill-Winter *et al.* [22] in the wind tunnel at the University of Melbourne discussed above, and velocity profile data were acquired using the same miniature hot-wire probes mentioned above. The wall shear was determined using a floating element force balance in the test wall at the most downstream station, and modified Clauser fits at other stations. The test wall was covered with P36 grit sandpaper with a roughness height (defined as six times the rms of the roughness) of 0.902 mm, resulting in fully rough conditions. The u_τ values determined for all of the rough wall profiles by the present method and by Squire *et al.* [4] are shown in Table III, and as with the smooth wall, the differences between the values from the two methods are small. A typical fit of the data is shown in Fig. 11. The result is similar to that of the smooth wall in Fig. 8.

With the u_τ values found using the present method, the roughness function, ΔU^+, can be determined at each profile location. The mean velocity in inner coordinates is shown in Fig. 12 for the same profile used in Fig. 11. The universal log law is shown using the same constants ($\kappa = 0.39$ and $A = 4.3$) used by Squire *et al.* [4]. Following the recommendation of Squire *et al.* [4] based on the work of Marusic *et al.* [23], the roughness function is taken as the average shift in the log law between the limits of $y^+ = 3.4\sqrt{\delta^+}$ and $0.19\delta^+$. For the profile of Fig. 12, $\Delta U^+ = 7.2$,

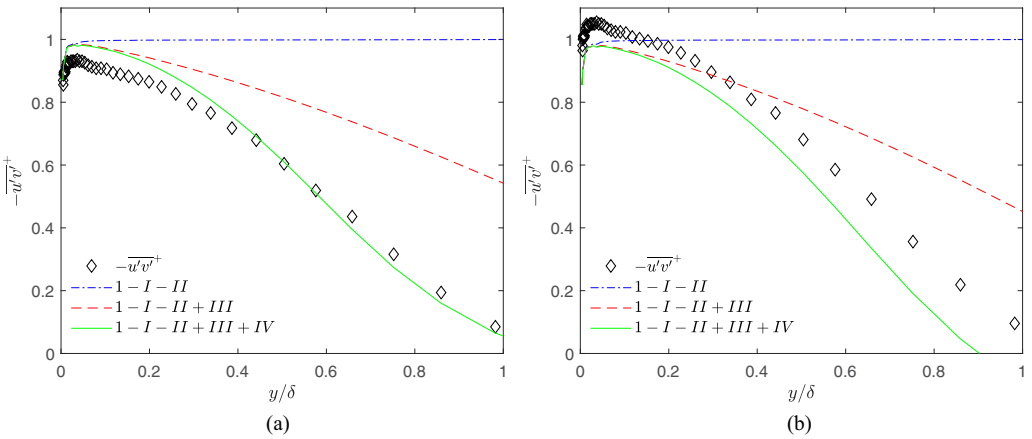

FIG. 10. Case of Fig. 8 with u_τ (a) increased by 3%, (b) decreased by 3%.

TABLE III. Comparison of u_τ and ΔU^+ found with present method and Clauser fit for rough wall ZPG cases of Squire *et al.* [4].

U_e [m/s]	x [m]	δ^+	u_τ [m/s] Present	u_τ [m/s] Clauser	u_τ diff. [%]	ΔU^+ Present	ΔU^+ Clauser	ΔU^+ diff.
7.3	7.0	2890	0.310	0.314	1.3	4.50	4.5	0
7.2	15.0	5190	0.289	0.290	0.3	4.10	4.2	−0.10
7.3	21.7	6770	0.284	0.288	1.4	3.92	4.2	−0.28
12.1	7.0	5250	0.524	0.529	0.9	6.24	6.3	−0.06
12.2	15.0	8980	0.501	0.503	0.4	6.04	6.1	−0.06
12.2	21.7	12300	0.489	0.488	0.2	5.74	6.0	−0.26
17.1	7.0	7670	0.752	0.754	0.3	7.44	7.4	0.04
17.4	15.0	13140	0.716	0.718	0.3	7.21	7.2	0.01
17.3	21.7	17190	0.692	0.698	0.9	6.97	7.1	−0.13

which matches the value reported by Squire *et al.* [4] based on the modified Clauser fit. Roughness functions for all locations are given in Table III.

Adverse pressure gradient cases were examined from the work of Marusic and Perry [24]. The experiments were done on a smooth wall in a smaller wind tunnel than in the cases discussed above, and conventional x-wire probes were used for the Reynolds shear stress measurements. Figure 13 shows a typical fit of the data. As in the laminar case of Fig. 1(c), there is no constant stress region. The dimensionless Reynolds shear stress rises from the wall to values above 1. Data were not available close enough to the wall to match the prediction using only terms I and II. With term III included, the data could be fit to about $y/\delta = 0.3$. With term IV included, the fit was good nearly to the edge of the boundary layer. Table IV shows results for all available stations and flow conditions. The u_τ values found with the present method average about 5% lower than those determined by Marusic and Perry [24] using the Clauser fit. While not an unreasonable difference, it is larger than observed in the ZPG cases above. The differences could be due to deficiencies in the present method or the Clauser fit, but there are no reasons to suspect either. The deceleration is sufficiently mild that the Clauser

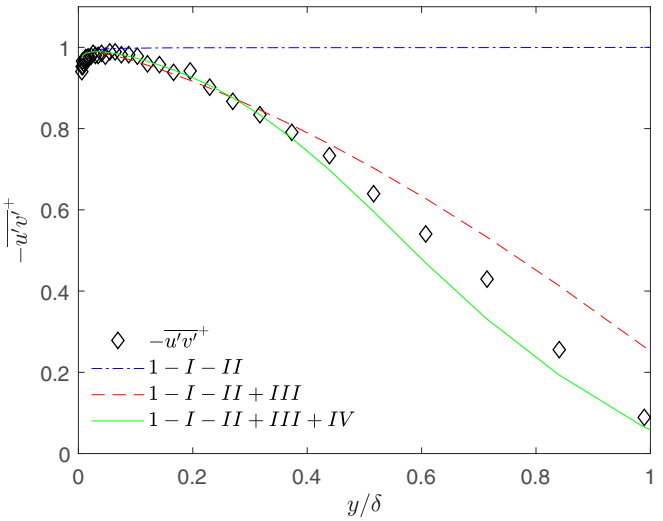

FIG. 11. Terms of Eq. (4) as indicated in legend for rough wall ZPG flow of Squire *et al.* [4], $x = 15.0\,\mathrm{m}$, $U_e = 17.4\,\mathrm{m/s}$, $\delta^+ = 13140$, $u_\tau = 0.716\,\mathrm{m/s}$.

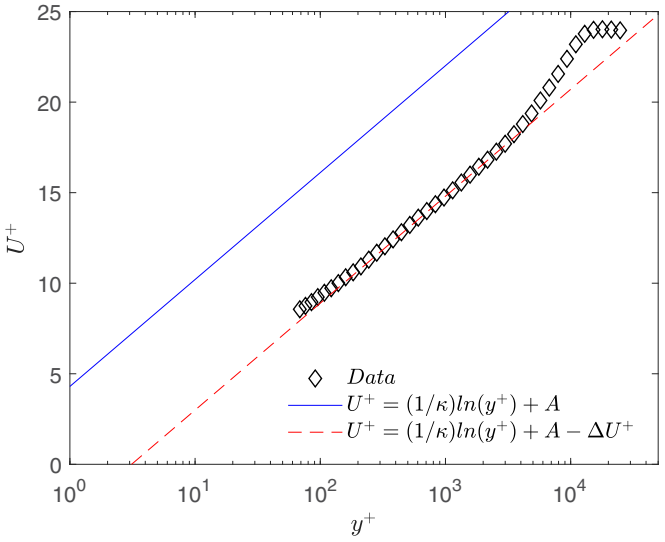

FIG. 12. Mean velocity for case of Fig. 11.

fit should be accurate. Another possibility is slightly low $-\overline{u'v'}$ data. Conventional x-wire probes are known to provide low values of the wall-normal component of the velocity, as explained by Champagne and Sleicher [25], who proposed a correction. For the hot-wire sensors used by Marusic and Perry [24], this correction results in an 8% increase in all $-\overline{u'v'}$ measurements. This correction was applied to the data, and the fits with the present method were done again. The corrected u_τ values are shown in Table IV. Agreement with the Clauser fit is better. The present method results are no longer biased below the Clauser fit values, and the average difference between methods is reduced to 2%.

The sink flow (FPG) study of Jones *et al.* [26] is considered next. As with the APG cases above, the Reynolds shear stress was measured with a conventional x-wire probe. The smooth wall boundary

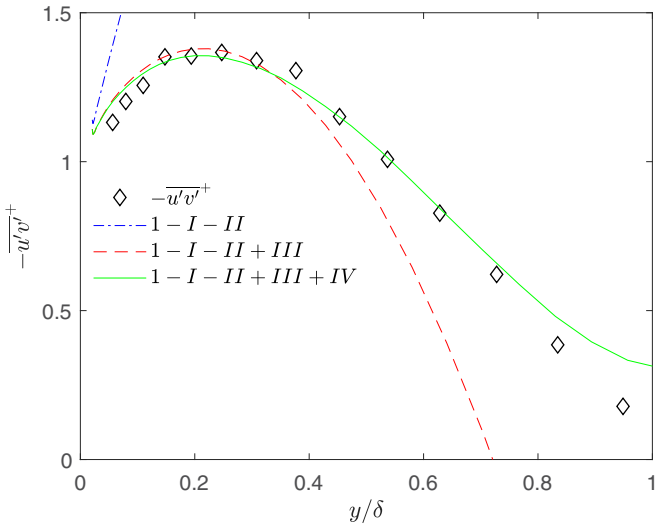

FIG. 13. Terms of Eq. (4) as indicated in legend for turbulent smooth wall APG flow of Marusic and Perry [24], $x = 2.24\,\mathrm{m}$, $U_e = 27.1\,\mathrm{m/s}$, $\delta^+ = 2810$, $K = -0.94 \times 10^{-7}$, $u_\tau = 0.905\,\mathrm{m/s}$.

TABLE IV. Comparison of u_τ found with present method and Clauser fit for smooth wall APG cases of Marusic and Perry [24]; uncor.: present method using $\overline{u'v'}$ as measured, corr.: present method with Champagne and Sleicher [25] correction applied.

U_e [m/s]	x [m]	$10^7\,K$	δ^+	u_τ [m/s] uncor.	u_τ [m/s] corr.	u_τ [m/s] Clauser	u_τ diff. [%]
10.4	1.20	0	792	0.419	0.440	0.441	−0.2
10.0	1.80	–2.14	1006	0.360	0.375	0.393	−4.6
9.3	2.24	–2.89	1072	0.317	0.335	0.331	1.2
8.6	2.64	–3.33	1135	0.257	0.273	0.273	0
8.2	2.88	–3.53	1162	0.225	0.244	0.237	3.0
7.9	3.08	–3.83	1156	0.188	0.203	0.207	−1.9
30.8	1.20	0	2150	1.180	1.220	1.166	4.6
29.1	1.80	–0.72	2536	0.960	1.000	1.031	3.0
27.1	2.24	–0.94	2810	0.860	0.905	0.900	0.6
25.2	2.64	–1.16	3055	0.720	0.750	0.766	−2.0
23.9	2.88	–1.21	3164	0.610	0.640	0.681	6.0
23.0	3.08	–1.33	3207	0.550	0.590	0.603	2.2

layer was allowed to develop with a zero pressure gradient, which was followed by acceleration with constant K. Figure 14(a) shows a typical fit of the data from a station where the flow is still developing. As in the APG cases, there is no constant stress region, but with the FPG the total shear stress drops rapidly from its value of 1 at the wall. Terms I and II are insufficient to match the Reynolds shear, but with term III included there is reasonable agreement to about $y/\delta = 0.3$. With term IV included, the fit matches the data to the edge of the boundary layer. Results for all stations at two different acceleration rates are shown in Table V. As with the APG cases of Table IV, the u_τ values from the present method are systematically low by about 3% compared to those obtained with the Clauser fit. If the Champagne and Sleicher [25] correction is applied to the experimental $-\overline{u'v'}$ data, u_τ values from the present method increase and agree with the Clauser fit results to within about 1%.

As noted in the comparison to the DNS results of Spalart [10], a sink flow boundary layer will eventually reach equilibrium after a sufficient development length. The terms $d\sqrt{c_f/2}/dx$ and $\partial U^+/\partial x$ go to zero, resulting in term IV equaling zero and simplifying the coefficient of term III

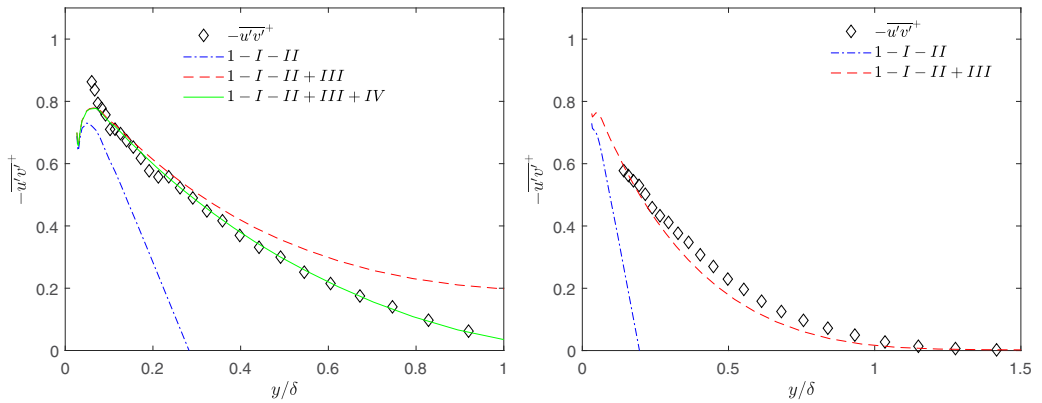

FIG. 14. Terms of Eq. (4) as indicated in legend for turbulent smooth wall FPG flow of Jones *et al.* [26], (a) $x = 2.20\,\text{m}, U_e = 9.0\,\text{m/s}, \delta^+ = 670, K = 5.39 \times 10^{-7}, u_\tau = 0.420\,\text{m/s}$; (b) $x = 3.58\,\text{m}, U_e = 15.06\,\text{m/s}, \delta^+ = 928, K = 5.39 \times 10^{-7}, u_\tau = 0.695\,\text{m/s}$.

TABLE V. Comparison of u_τ found with present method and Clauser fit for smooth wall FPG cases of Jones *et al.* [26]; uncor.: present method using $\overline{u'v'}$ as measured, corr.: present method with Champagne and Sleicher [25] correction applied.

U_e [m/s]	x [m]	$10^7\ K$	δ^+	u_τ [m/s] uncor.	u_τ [m/s] corr.	u_τ [m/s] Clauser	u_τ diff. [%]
12.00	0.80	2.70	632	0.535	0.550	0.551	−0.2
14.74	1.60	2.70	914	0.630	0.650	0.658	−1.2
17.46	2.20	2.70	1102	0.755	0.775	0.770	0.6
21.45	2.80	2.70	1293	0.915	0.940	0.940	0
25.63	3.28	2.70	1427	1.100	1.130	1.116	1.2
30.57	3.58	2.70	1582	1.330	1.330	1.329	0.1
6.09	0.80	5.39	388	0.268	0.273	0.302	−9.6
7.54	1.60	5.39	567	0.347	0.358	0.362	−1.1
9.00	2.20	5.39	670	0.413	0.420	0.427	−1.6
11.00	2.80	5.39	784	0.509	0.520	0.516	0.8
13.10	3.28	5.39	873	0.595	0.617	0.610	1.1
15.06	3.58	5.39	928	0.695	0.695	0.701	−0.9

in Eq. (4). The fit of Eq. (4) is shown in Fig. 14(b) for a downstream station of the Jones *et al.* [26] study, where sink flow similarity had been achieved. There is good fit of the $-\overline{u'v'}^+$ data. It is interesting to note that u_τ can in theory be found with the present method without need of the $-\overline{u'v'}$ data. The correct u_τ is the one which causes the right side of Eq. (4) to asymptote to zero at large y. Experimental uncertainty prevents this from happening in the general case, but with Eq. (4) simplified for the equilibrium sink flow, it can be done reliably.

VII. DISCUSSION

As with all methods, the present formulation has both advantages and disadvantages. The present method, the momentum integral method, and the method of Mehdi *et al.* [17], for example, are based on exact representations of the boundary layer momentum equation. Supplied with perfect data (or DNS results) they will all produce exactly the same correct answer. Given real experimental data, their performance depends on the terms that must be computed, the influence of experimental uncertainty on these terms, and the parts of the boundary layer where accurate results are most required. The momentum integral method, for example, has the advantage of requiring no turbulence data, but does require sufficient near wall data to accurately compute the momentum thickness and sufficient streamwise resolution to determine $\partial\theta/\partial x$. Brzek *et al.* [11] successfully used the momentum integral method and emphasized the need to obtain $\partial\theta/\partial x$ accurately. They also obtained u_τ for a ZPG profile using the equivalent of Eq. (3), where again good streamwise resolution was needed to compute $\partial U/\partial x$ accurately. The method of Mehdi *et al.* [17] has different requirements. It requires the Reynolds shear stress profile, but only at one location since no streamwise gradients are needed. It requires data sufficiently accurate to compute the wall normal gradient of the total shear stress, which they found requires smoothing and fitting of the data to expected profile shapes in the near wall region.

For the present method, the requirements are different. Reynolds shear stress data are required, and data from at least two streamwise locations are needed to estimate streamwise gradients. The importance of the accuracy of these gradients has been reduced, however, by the transformation of the equation into wall coordinates. An advantage of the method is that it does not require any particularly specialized equipment such as force balances or probes for acquiring velocity data exceptionally close to a surface. It only requires profiles of the mean streamwise velocity and the Reynolds shear stress at two or more locations, which are already typically acquired in many boundary layer studies. No

presumption is made about the shape of the mean velocity profile, as is necessary with techniques such as the Clauser fit or Preston tube measurements.

Given the differences in measurement requirements, the choice of method to determine u_τ depends on the flow in question and the data acquired from the available instrumentation. No single method should be expected to be best in all cases. For fully developed turbulent boundary layers, the Clauser fit remains a simple and preferred method for most zero pressure gradient cases. It depends, however, on the universal law of the wall. The present method can be used in arbitrary pressure gradients where significant deviations from the log law are present. Fitting of the Reynolds shear stress profile can be done in any part of the boundary layer. Data from very near the wall and gradients of the Reynolds or total shear, which can be difficult to obtain accurately, are not required. It is also unnecessary to rely on results from the outer part of the boundary where streamwise gradient terms become more significant and can cause error. Instead, focus can be on the middle of the boundary layer where all terms are typically known with more certainty.

VIII. CONCLUSIONS

An analytical method has been developed for relating mean velocity and Reynolds shear stress profiles, and this method has been used to determine the wall shear stress from measured profile data. The method is applicable for steady, two-dimensional boundary layers with arbitrary pressure gradients and surface roughness. It utilizes the boundary layer streamwise momentum equation, which is transformed into inner coordinates without approximation. The accuracy of the method was demonstrated and the relative importance of the terms in the formulation determined through application to laminar flow solutions and turbulent DNS results. The utility of the method was shown through application to experimental data from the literature including zero pressure gradient cases from smooth and rough walls and smooth wall cases with favorable and adverse pressure gradients. Results obtained with the present method agreed closely with those obtained by other methods in the original studies.

ACKNOWLEDGMENTS

The authors would like to thank the Office of Naval Research for providing financial support under Grant No. N0001417WX00756, and Prof. Ivan Marusic and Dr. Dougal Squire of the University of Melbourne for providing tabulated experimental data for Refs. [4,21,22,24,26]. Tabulated DNS data were obtained from the databases available on the websites of the Fluid Dynamics Group of the Universidad Politécnica de Madrid, and the ERCOFTAC site maintained at the University of Manchester. The authors also thank the referees, whose insightful questions and recommendations helped improve the paper.

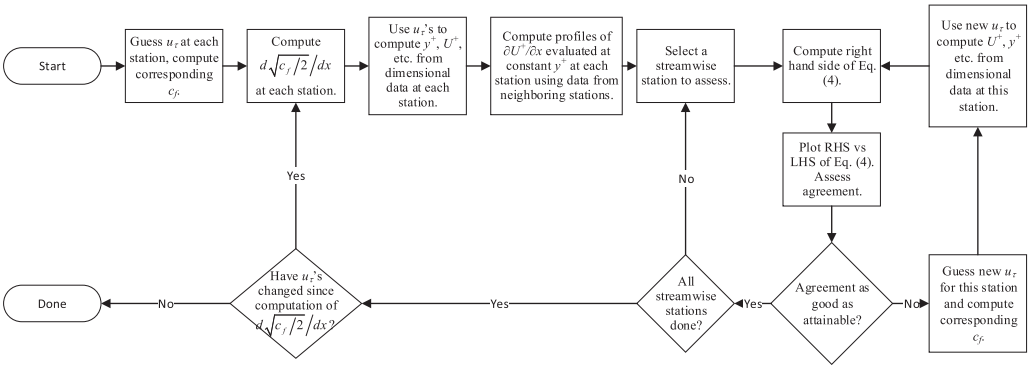

FIG. 15. Flow chart showing iterative method for finding u_τ.

APPENDIX

The above flow chart (Fig. 15) shows the implementation of the iterative method for finding the wall shear.

[1] K. G. Winter, An outline of the techniques available for the measurement of skin friction in turbulent boundary layers, Prog. Aerosp. Sci. **18**, 1 (1979).

[2] J. H. Haritonidis, The measurement of wall shear stress, Adv. Fluid Mech. Meas. **40**, 229 (1989).

[3] J. C. Klewicki, W. S. Saric, I. Marusic, and J. K. Eaton, Wall-bounded flows, in *Springer Handbook of Experimental Fluid Mechanics*, edited by C. Tropea, A. L. Yarin, and J. F. Foss (Springer-Verlag, Berlin, 2007), p. 875.

[4] D. T. Squire, C. Morrill-Winter, N. Hutchins, M. P. Schultz, J. C. Klewicki, and I. Marusic, Comparison of turbulent boundary layers over smooth and rough surfaces up to high Reynolds numbers, J. Fluid Mech. **795**, 210 (2016).

[5] J. W. Naughton and M. Sheplak, Modern developments in shear stress measurements, Prog. Aerosp. Sci. **38**, 515 (2002).

[6] S. A. Dixit and O. N. Ramesh, Pressure-gradient-dependent logarithmic laws in sink flow turbulent boundary layers, J. Fluid Mech. **615**, 445 (2008).

[7] F. Clauser, Turbulent boundary layers in adverse pressure gradients, J. Aero. Sci. **21**, 91 (1954).

[8] M. P. Schultz and K. A. Flack, The rough-wall turbulent boundary layer from the hydraulically smooth to the fully rough regime, J. Fluid Mech. **580**, 381 (2007).

[9] W. P. Jones and B. E. Launder, Some properties of sink flow turbulent boundary layers, J. Fluid Mech. **56**, 337 (1972).

[10] P. R. Spalart, Numerical study of sink-flow boundary layers, J. Fluid Mech. **172**, 307 (1986).

[11] B. Brzek, R. B. Cal, G. Johansson, and L. Castillo, Inner and outer scalings in rough surface zero pressure gradient turbulent boundary layers, Phys. Fluids **19**, 065101 (2007).

[12] K. Fukagata, K. Iwamoto, and N. Kasagi, Contribution of Reynolds stress distribution to the skin friction in wall-bounded flows, Phys. Fluids **14**, L73 (2002).

[13] S. Deck, N. Renard, R. Laraufie, and P. E. Weiss, Large-scale contribution to mean wall shear stress in high-Reynolds-number flat-plate boundary layers up to $\mathrm{Re}_\theta = 13650$, J. Fluid Mech. **743**, 202 (2014).

[14] M. Yoon, J. Ahn, J. Hwang, and H. J. Sung, Contribution of velocity-vorticity correlations to the frictional drag in wall-bounded turbulent flows, Phys. Fluids **28**, 081702 (2016).

[15] N. Renard and S. Deck, A theoretical decomposition of mean skin friction generation into physical phenomena across the boundary layer, J. Fluid Mech. **790**, 339 (2016).

[16] F. Mehdi and C. M. White, Integral form of the skin friction coefficient suitable for experimental data, Exp. Fluids **50**, 43 (2011).

[17] F. Mehdi, T. G. Johansson, C. M. White, and J. W. Naughton, On determining wall shear stress in spatially developing two-dimensional wall-bounded flows, Exp. Fluids **55**, 1656 (2014).

[18] V. M. Falkner and S. W. Skan, Some approximate solutions of the boundary layer equations, Phil. Mag. **12**, 865 (1931).

[19] J. Jiménez, S. Hoyas, M. P. Simens, and Y. Mizuno, Turbulent boundary layers and channels at moderate Reynolds numbers, J. Fluid Mech. **657**, 335 (2010).

[20] J. A. Sillero, J. Jiménez, and R. D. Moser, One-point statistics for turbulent wall-bounded flows at Reynolds numbers up to $\delta^+ \approx 2000$, Phys. Fluids **25**, 105105 (2013).

[21] C. Morrill-Winter, J. Klewicki, R. Baidya, and I. Marusic, Temporally optimized spanwise vorticity sensor measurements in turbulent boundary layers, Exp. Fluids **56**, 216 (2015).

[22] C. Morrill-Winter, D. T. Squire, J. C. Klewicki, N. Hutchins, M. P. Schultz, and I. Marusic, Reynolds number and roughness effects on turbulent stresses in sandpaper roughness boundary layers, Phys. Rev. Fluids **2**, 054608 (2017).

[23] I. Marusic, J. P. Monty, M. Hultmark, and A. J. Smits, On the logarithmic region in near wall turbulence, J. Fluid Mech. **716**, R3 (2013).
[24] I. Marusic and A. E. Perry, Review of hydraulic roughness scales in the fully rough regime, J. Fluid Mech. **298**, 389 (1995).
[25] F. H. Champagne and C. A. Sleicher, Turbulence measurements with inlined hot-wire. Part 2. Hot-wire response equations, J. Fluid Mech. **28**, 177 (1967).
[26] M. B. Jones, I. Marusic, and A. E. Perry, Evolution and structure of sink-flow turbulent boundary layers, J. Fluid Mech. **428**, 1 (2001).